

Point-contact spectroscopy on antiferromagnetic Kondo semiconductors CeT_2Al$_{10}$ (T=Ru and Os)

Jie Li(李洁), Li-Qiang Che(车利强), Tian Le(乐天), Jia-Hao Zhang(张佳浩), Pei-Jie Sun(孙培杰), Toshiro Takabatake, Xin Lu(路欣)

Citation: Chin. Phys. B . 2020, 29(7): 077103 . **doi:** 10.1088/1674-1056/ab8dab
Journal homepage: http://cpb.iphy.ac.cn; http://iopscience.iop.org/cpb

What follows is a list of articles you may be interested in

Point-contact spectroscopy on antiferromagnetic Kondo semiconductors CeT_2Al$_{10}$ (T=Ru and Os)

Jie Li(李洁), Li-Qiang Che(车利强), Tian Le(乐天), Jia-Hao Zhang(张佳浩), Pei-Jie Sun(孙培杰), Toshiro Takabatake, Xin Lu(路欣)
Chin. Phys. B . 2020, 29(7): 077103 . **doi:** 10.1088/1674-1056/ab8dab

Lifshitz transition in triangular lattice Kondo-Heisenberg model

Lan Zhang(张欄), Yin Zhong(钟寅), Hong-Gang Luo(罗洪刚)
Chin. Phys. B . 2020, 29(7): 077102 . **doi:** 10.1088/1674-1056/ab8da4

Giant topological Hall effect of ferromagnetic kagome metal Fe_3Sn_2

Qi Wang(王琦), Qiangwei Yin(殷蔷薇), Hechang Lei(雷和畅)
Chin. Phys. B . 2020, 29(1): 017101 . **doi:** 10.1088/1674-1056/ab5fbc

Possible nodeless $s^{\pm}$-wave superconductivity in twisted bilayer graphene

Zhe Liu(刘哲), Yu Li(李宇), Yi-Feng Yang(杨义峰)
Chin. Phys. B . 2019, 28(7): 077103 . **doi:** 10.1088/1674-1056/28/7/077103

Antiferromagnetism and Kondo screening on a honeycomb lattice

Lin Heng-Fu, Tao Hong-Shuai, Guo Wen-Xiang, Liu Wu-Ming
Chin. Phys. B . 2015, 24(5): 057101 . **doi:** 10.1088/1674-1056/24/5/057101

Point-contact spectroscopy on antiferromagnetic Kondo semiconductors CeT_2Al_{10} (T = Ru and Os)*

Jie Li(李洁)[1], Li-Qiang Che(车利强)[1], Tian Le(乐天)[1], Jia-Hao Zhang(张佳浩)[2], Pei-Jie Sun(孙培杰)[2], Toshiro Takabatake[1,3], and Xin Lu(路欣)[1,4,5,†]

[1] *Center for Correlated Matter and Department of Physics, Zhejiang University, Hangzhou* 310058, *China*
[2] *Institute of Physics, Chinese Academy of Sciences, Beijing* 100190, *China*
[3] *Department of Quantum Matter, ADSM, Hiroshima University, Higashi-Hiroshima,* 739-8530, *Japan*
[4] *Zhejiang Province Key Laboratory of Quantum Technology and Device, Zhejiang University, Hangzhou* 310027, *China*
[5] *Collaborative Innovation Center of Advanced Microstructures, Nanjing University, Nanjing* 210093, *China*

(Received 20 March 2020; revised manuscript received 22 April 2020; accepted manuscript online 28 April 2020)

We have carried out point-contact spectroscopy (PCS) measurements on one family of antiferromagnetic Kondo semiconductor CeT_2Al_{10} (T = Ru and Os) with a Néel temperature $T_N \sim 27.5$ and 28.5 K, respectively. Their PCS conductance curves both exhibit a characteristic coherent double-peak-structure at temperatures below T_N, signaling an AFM gap around the Fermi surface. The temperature dependent AFM gap Δ_1 follows a Bardeen–Cooper–Schrieffer (BCS)-like mean-field behavior with a moderate gap anisotropy for PCS along different crystal axes. Another asymmetric gap-like feature is observed for both compounds at temperatures far below T_N, which is consistent with opening of a new hybridization gap Δ_h inside the long-range ordered AFM state. Our results suggest a common itinerant nature of the anomalous AFM ordering, constraining theoretical models to explain the AFM origin in $CeRu_2Al_{10}$ and $CeOs_2Al_{10}$.

Keywords: point-contact spectroscopy, Kondo semiconductor, antiferromagnetism, hybridization gap

PACS: 71.27.+a, 75.20.Hr **DOI:** 10.1088/1674-1056/ab8dab

1. Introduction

As a typical strongly-correlated electron system, heavy fermions have attracted intensive attention because of their rich phase diagrams and exotic quantum states such as antiferromagnetism (AFM), superconductivity, and non-Fermi-liquid behavior, where the ground states are tuned by the delicate competition between the Ruderman–Kittel–Kasuya–Yosida (RKKY) and Kondo interactions. A small number of rare-earth based heavy fermion systems exhibit insulating or semiconducting behaviors, thus called Kondo insulator or semiconductor.[1] Their Fermi level E_F sits right inside the gap formed by hybridization between the localized f and conduction electrons, and the local f moments are generally screened by the conduction electrons with Kondo interactions in a paramagnetic state. For example, the ground state of $CeFe_2Al_{10}$ is semiconducting and paramagnetic.[2,3] However, its isoelectronic counterparts CeT_2Al_{10} (T = Ru and Os) exhibit an unexpected high Néel temperature $T_N = 27.5$ K and 28.5 K, respectively. μSR and neutron diffraction measurements have confirmed the AFM order in $CeRu_2Al_{10}$ with a propagation vector $\boldsymbol{K} = (0,1,0)$,[4–8] and the ordered magnetic moment μ_{AF} ($\simeq 0.3\ \mu_B$/Ce in $CeOs_2Al_{10}$ and $0.4\ \mu_B$ in $CeRu_2Al_{10}$) is aligned along the c-axis rather than the crystalline electric field (CEF) easy a-axis, indicating a strong anisotropy of the hybridization interactions.[9,10]

The CeT_2Al_{10} (T = Fe, Ru, and Os) family crystallizes in an orthorhombic crystal structure of $YbFe_2Al_{10}$-type (*cmcm*, $Z = 4$)[11] instead of the well-known tetragonal $ThMn_{12}$-type.[12] In the unit cell, each Ce atom is situated in a polyhedral cage, consisting of 16 Al atoms and 4 Ru (or Os) atoms and leading to the shortest Ce–Ce distance longer than 5.2 Å. In comparison, its Gd counterpart $GdRu_2Al_{10}$ has an AFM order below $T_N = 18$ K with an ordered moment of 7 μ_B/Gd. If the magnetic transition temperatures for rare-earth compounds are assumed to follow the scaling law of their de Gennes factors,[13–15] the expected Néel temperature in $CeRu_2Al_{10}$ is estimated to be only 0.2 K, nearly 100 times smaller than the actual value, arguing against the local origin of the AFM order due to RKKY interactions but favoring an itinerant character of Ce f electrons in CeT_2Al_{10} instead. The optical studies observed a formation of CDW-like gap along b-axis, probably essential to the abnormal AFM states in both $CeRu_2Al_{10}$ and $CeOs_2Al_{10}$.[16,17] In recent uniaxial pressure experiments, the distance of the Ce–T (T = Ru and Os) along the b axis may be a key parameter to tune T_N.[18] The magneto-transport study of $CeRu_2Al_{10}$ suggests an enhanced Nernst coefficient $S(T)$ for its thermoelectric response, similar to the mysterious hidden order in URu_2Si_2.[19] Despite of these efforts,[18,20,21]

*Project supported by the National Key Research and Development Program of China (Grant Nos. 2017YFA0303101 and 2016FYA0300402), the National Natural Science Foundation of China (Grant Nos. 11674279, 11774404, and 11374257), the Zhejiang Provincial Natural Science Foundation of China (Grant No. LR18A04001), and the Japan Society for the Promotion of Science KAKENHI (Grant Nos. JP26400363, JP16H01076, and JP17K05545).

†Corresponding author. E-mail: xinluphy@zju.edu.cn

© 2020 Chinese Physical Society and IOP Publishing Ltd

the mechanism of this unusual AFM order in CeT_2Al_{10} still remains elusive. Point-contact spectroscopy (PCS) can thus serve as a powerful tool to investigate the systematic evolution of the electronic density of states (DOS) across the AFM transition.[22–24]

In this paper, we have applied point-contact spectroscopy technique to study the high quality $CeRu_2Al_{10}$ and $CeOs_2Al_{10}$ single crystals. In both compounds, we have observed two sets of double-peak features at low temperatures far below T_N: One set of double-peak spectra is probably associated with an AFM gap Δ_1, following a mean-field-like temperature behavior, while the other set is likely to be an emergent hybridization gap Δ_h between f and conduction electrons inside the AFM state.

2. Experimental methods

$CeRu_2Al_{10}$ and $CeOs_2Al_{10}$ single crystals were grown with the Al self-flux method as described elsewhere.[18,19] Their resistance R and specific heat C/T vs. temperature T are shown in Figs. 1(a) and 1(b), respectively. The sharp upturns in resistivity and specific heat signal the AFM transition at $T_N = 27.5$ K and 28.5 K for $CeRu_2Al_{10}$ and $CeOs_2Al_{10}$, confirming the high crystal quality as reported. Single crystals from the same batch were broken at room temperature to expose fresh crystal surfaces and then Pt wires were immediately attached on the sample surface with a small drop of conductive silver paint with the averaged Ag grain size ~ 5 μm, where hundreds of parallel channels between the Ag grains and sample can be assumed and each channel has a much smaller contact area than the total silver paint size around 50–100 μm. This so-called "soft" point-contact method has an advantage of good mechanical and thermal stability against vibrations.[24] The conductance curves $G(V)$ were recorded with the conventional lock-in technique in a quasi-four-probe configuration, where the sample was always biased positively. The sample was cooled down to 1.8 K and a magnetic field up to 10 T was applied by the Quantum Design PPMS. The exposed surface orientations were later identified by the Laue x-ray diffraction patterns.

3. Results and discussion

Dozens of contacts have been measured on $CeRu_2Al_{10}$ and $CeOs_2Al_{10}$ single crystals, and the resistance of all contacts is in the range of 5–20 Ω. We have to stress that the contact size d should be in the ballistic limit compared with their electronic mean free path l, critical to guarantee the spectroscopic nature of the measured conductance curves. Despite the large 'footprint' of the Ag paint with a size around 50–100 μm, hundreds of effective contacts occur in a much smaller region due to the presence of parallel microbridges between the Ag particles and sample. The overall contact area can be estimated by the contact resistance R according to the Sharvin formula[25]

$$R(T) = \frac{16\rho l}{3\pi d^2}, \tag{1}$$

where ρ is the resistivity (~ 2 mΩ·cm), and l is the electron mean free path at low temperatures (~ 4 nm). Even though the total contact size d is estimated to be 106 nm with the averaged contact resistance around 12 Ω, we have to consider the fact that the averaged contact size d_0 for each channel of the point-contact junction can be $d_0 \sim d/N$ with N being the number of channels and it is likely that d_0 would still be much smaller than the electron mean free path l. In addition, we note that the contact resistance at high bias-voltage does not change with temperature up to 30 K and that the zero-bias contact resistance as a function of temperature $G_0^{-1}(T)$ in Fig. 1(c) resembles its respective electrical resistivity behavior in Fig. 1(a), ensuring the ballistic nature of our contacts.

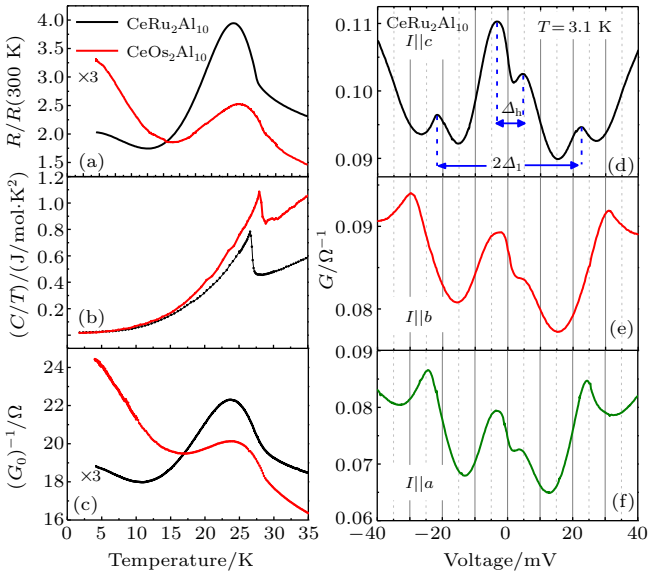


Fig. 1. Temperature dependence of (a) resistance, (b) specific heat C/T, and (c) point-contact zero-bias resistance $G_0^{-1}(T)$ for both $CeRu_2Al_{10}$ and $CeOs_2Al_{10}$ samples. (d)–(f) Point-contact conductance curves $G(V)$ of $CeRu_2Al_{10}$ at 3.1 K along c, b, and a axes, respectively.

Figures 1(d)–1(f) show three representative differential conductance curves $G(V)$ at 3.1 K for contacts on $CeRu_2Al_{10}$ crystals roughly along three principal axes c, b, and a, respectively. They all display an asymmetric double-peak structure around $\Delta_h \approx 9$ mV (peak to peak distance in Fig. 1(d) as defined in Refs. [26,27]) and another symmetric double-peak feature Δ_1 at around ±25 mV, 30 mV, and 23 mV along a-, b-, and c-axis (half of the peak-to-peak distance in Fig. 1(d) as in the superconductor case), respectively, showing a moderate gap anisotropy. Here, the symmetric double-peak structure displays two characteristic peaks near the gap edges above and below the Fermi energy and depleted density of states inside the gap similar to the superconducting coherence peak, where

its peak position is simply taken as the corresponding gap value Δ_1 (we would refer the symmetric double-peak structure as the Δ_1 coherence peaks hereafter). We note that the double-peaks at Δ_1 for $I \parallel c$ are relatively weak in intensity compared with other directions, probably implying the two-dimensional nature of the Fermi surface associated with the gap Δ_1. The temperature evolution of point-contact spectra $G(V)$ of $CeRu_2Al_{10}$ is shown in Fig. 2(a) from 3.5 K to 30.0 K, with the contact along the b-axis crystal orientation. As the temperature increases from 3.5 K, the asymmetric double-peak feature Δ_h evolves into a zero-bias conductance peak (ZBCP) and is barely noticeable at around 21–22 K, while the symmetric double-peak Δ_1 shifts to smaller bias-voltages and the Δ_1 coherence peaks are smeared in intensity and disappear at $T > 25.0$ K. A V-shape background is observed at 30.0 K above T_N probably due to the Kondo semiconducting gap around the Fermi surface.[28] For $CeRu_2Al_{10}$, the temperature dependent Δ_1 gap magnitude in Fig. 2(a) is plotted in Fig. 2(c) in comparison with the Δ_1 gap values in other directions. They all follow a BCS mean-field temperature behavior and the gap closes exactly at the Néel temperature $T_N \sim 27.5$ K for $CeRu_2Al_{10}$. We would thus attribute Δ_1 to the AFM gap below T_N, where the largest AFM gap in the b-axis with the smallest AFM intensity in the c-axis for PCS is consistent with the AFM propagation vector along $\boldsymbol{K} = (0,1,0)$ with the magnetic moment in the c-axis. In addition, we notice that a kink feature at Δ_2 develops in the conductance curve $G(V)$ below T_N as marked by the arrows in Fig. 2(a), suggesting a depleted density of states with the AFM transition in contrast to the Δ_1 coherence peak structure. This kink feature gets more pronounced in another set of $G(V)$ curves as shown in Fig. 2(b) and its voltage position Δ_2 as a function of temperature also follows the mean-field behavior, whose exact origin requires further careful studies.

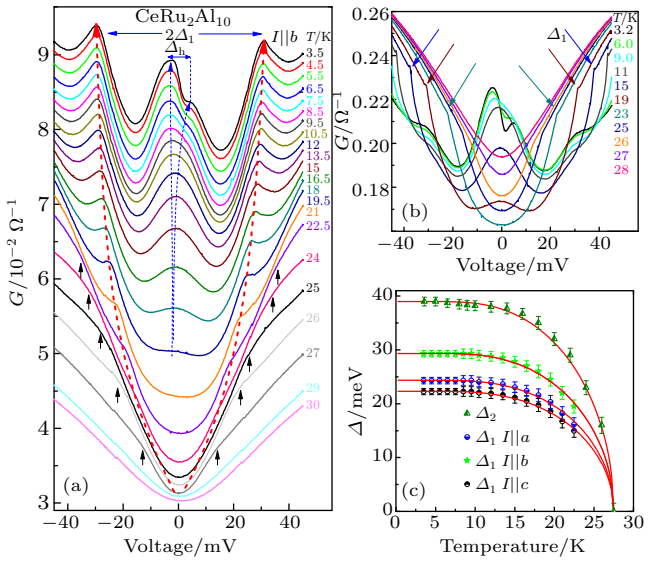


Fig. 2. (a) and (b) The temperature evolution of soft point-contact conductance curves $G(V)$ as a function of the biased voltage for $CeRu_2Al_{10}$ with surface along b axis and an arbitrary direction, respectively. The curves are vertically shifted for clarity and the dashed lines are a guide for eyes to show the temperature evolution of the AFM gap Δ_1 and hybridization gap Δ_h, respectively. The arrows mark the position of the kink structure Δ_2 in the conductance curve $G(V)$. (c) Temperature dependence of the extracted AFM gap Δ_1 for $CeRu_2Al_{10}$ in three crystallographic orientations in comparison with the standard mean-field BCS curves and the Δ_2 value for the kink structure also follows the BCS behavior.

The asymmetric double-peak feature of $CeRu_2Al_{10}$ below T_N is characteristic of an emergent hybridization gap $\Delta_h \sim 9$ meV at 3.2 K, similar to the asymmetric double-peaks for PCS on URu_2Si_2 and UPd_2Al_3.[29] It probably roots in the modified hybridization between f–c electrons due to the presence of AFM ordering below T_N, yielding a metallic state coexisting with the Kondo semiconducting behaviors. We note that the resistivity below T_N in $CeRu_2Al_{10}$ is not divergent with decreased temperature as for a typical Kondo semiconductor. In order to quantitatively analyze the hybridization gap Δ_h for $CeRu_2Al_{10}$ in (001) direction, a co-tunneling model has been adopted to fit the point-contact conductance curves, which has been proven effective in the case of URu_2Si_2 and UPd_2Al_3. Distinct from the general Fano shape in a single Kondo impurity model,[30] a double-peak resonance separated by a narrow hybridization gap Δ_h is observed instead.[26,27] Our model formula is $G(eV) = \mathrm{Im}\widetilde{G}^{\mathrm{KL}}_{\psi}(eV) + \eta G_0(eV)$, where the first term is the Fano conductance while the second term accounts for the background shape with η as a weighting factor. Figure 3(a) shows one set of $G(V)$ curves for PCS on $CeRu_2Al_{10}$ along the (001) direction in comparison with their optimal fittings on a parabolic background. A hybridization gap $\Delta_h = 9$ meV is obtained for $CeRu_2Al_{10}$ at 3.0 K. Its temperature dependence is plotted in Fig. 3(b), and the extracted Δ_h decreases linearly with increasing temperature between 3 K and 19 K, which is in contrast to the BCS-like temperature dependence of Δ_1. A linear extrapolation of Δ_h terminates at approximately 32.5 K, slightly higher than its T_N. Figure 3(c) shows the conductance curves $G(V)$ in different magnetic fields at 1.8 K, where the peak height is gradually suppressed in field but without any obvious change of the peak position.

Figures 4(a)–4(c) show the normalized conductance curves $G(V)$ for different $CeOs_2Al_{10}$ surfaces at 3.0 K, and G_N is the point-contact conductance normalized by the conductance at the highest bias voltage. It is difficult to identify their exact surface orientations due to the limitation of crystal size. In addition to a pronounced parabolic background, the $G(V)$ curves show a similar symmetric double-peak feature associated with the gap Δ_1 in the range of 35–50 mV for different surfaces. At the lower bias-voltage, a symmetric gap-like shoulder feature Δ_h around ± 10 mV is commonly observed with more depleted DOS around zero bias, distinguishing itself from that of $CeRu_2Al_{10}$.

The temperature evolution of point-contact spectra $G(V)$ on $CeOs_2Al_{10}$ from 1.8 K to 30.0 K is shown in Fig. 4(d). With increasing temperature, the shoulder-like gap feature Δ_h

smoothly shifts to smaller bias-voltages and disappears at temperatures above 17 K, while the Δ_1 symmetric double-peaks move to lower bias-voltages and become barely detectable at $T > 27$ K. $CeOs_2Al_{10}$ also shows a V-sharp background at temperatures above T_N, consistent with its Kondo semiconductor nature. If we still simply take the Δ_1 peak position as its gap value, the temperature dependence of the AFM gap Δ_1 is plotted in Fig. 4(e) in comparison with the BCS curves. It is clear that the gap Δ_1 in $CeOs_2Al_{10}$ also follows the mean-field BCS behavior similar to $CeRu_2Al_{10}$ and it is reasonable to be identified as the associated AFM gap. The shoulder-like gap feature can only be observed at temperatures far below T_N and the dip between the Δ_1 double-peaks becomes flat at the intermediate temperature, corresponding to the kink at 17 K in the temperature-dependent zero-bias conductance curve $G_0(T)$ as in Fig. 4(f). Even though the shoulder-like feature in $CeOs_2Al_{10}$ should have a common origin as in $CeRu_2Al_{10}$, most likely due to the new hybridization gap Δ_h, this gap Δ_h opened at much lower temperatures than T_N seems irrelevant or at least a secondary effect of the AFM transition in $CeOs_2Al_{10}$.

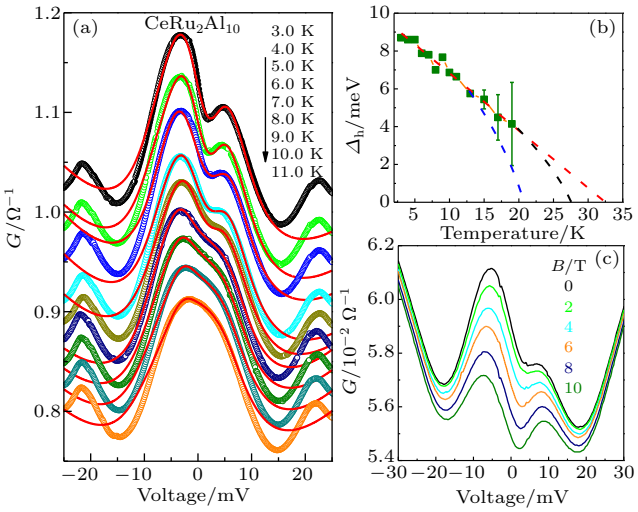


Fig. 3. (a) Co-tunneling fitting curves (solid lines) in comparison with the temperature dependent conductance curves $G(V)$ (circles). The curves are shifted for clarity. (b) The extracted hybridization gap Δ_h as a function of temperature from the co-tunneling model fitting (solid squares). A linear extrapolation of the gap closes at 32.5 K (red dashed line) and the black dashed line starts around T_N. (c) The point-contact conductance curves $G(V)$ as a function of magnetic field B up to 10 T at $T = 1.8$ K.

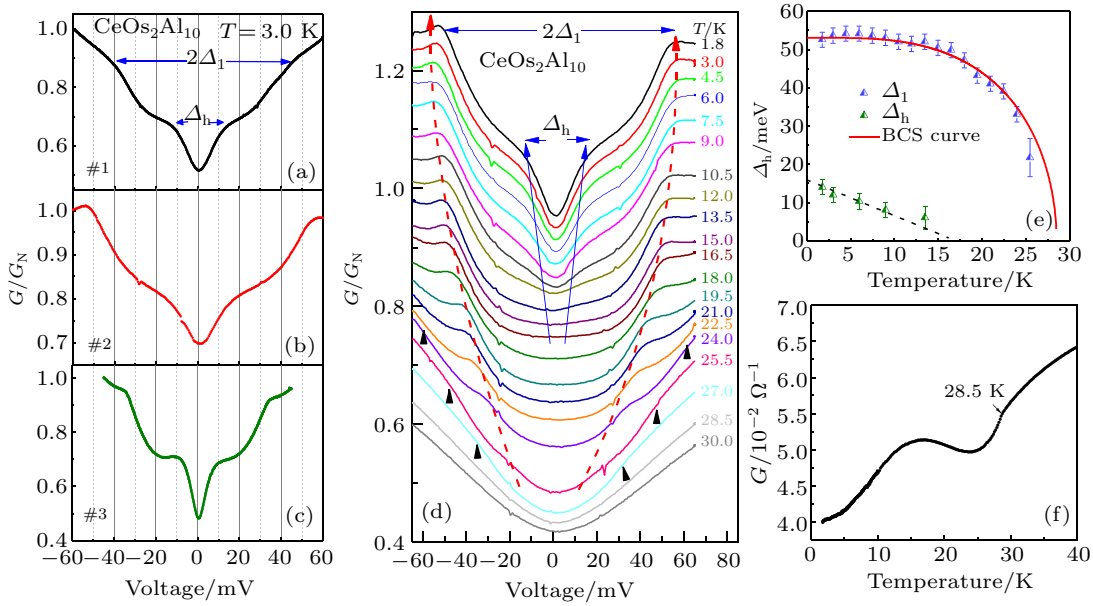


Fig. 4. (a)–(c) The $G(V)$ of $CeOs_2Al_{10}$ at 3.0 K on different cyrstal surfaces. (d) The temperature evolution of the soft point-contact conductance curves $G(V)$ as a function of the biased voltage for $CeOs_2Al_{10}$. The curves are vertically shifted for clarity and the dashed lines are a guide for eyes to show the temperature evolution of the AFM gap Δ_1 and hybridization gap Δ_h, respectively. The arrows mark the position of the kink structure Δ_2 in the conductance curve $G(V)$. (e) Temperature dependence of the extracted AFM gap Δ_1 for $CeOs_2Al_{10}$ in comparison with the standard mean-field BCS curves and the estimated hybridization gap Δ_h. (f) Zero-bias conductance curve as a function of temperature $G_0(T)$ up to 40 K for a point-contact on $CeOs_2Al_{10}$.

When comparing the conductance curves $G(V)$ between $CeRu_2Al_{10}$ and $CeOs_2Al_{10}$, both V-shape backgrounds for temperature above T_N comply with the Kondo semiconductor behavior and the symmetric coherence peaks below T_N can be commonly identified as the AFM gap. Similar gaped structure has been reported in optical conductivity[16,17] and break junction tunneling measurements,[31,32] where an AFM gap also develops around T_N and follows the typical mean-field temperature behavior. However, we notice that the reported gap for optical conductivity in $CeOs_2Al_{10}$ develops below 36 K far above its $T_N = 28.5$ K and is manifested as a peak at 20 meV. The temperature behavior of the AFM gap in break-junction studies on $CeOs_2Al_{10}$ is similar to our PCS results and its gap value $\Delta_{AF} \sim 50$–60 meV (Δ_1 in our case) seems comparable to ours. The exact origin of the difference among different techniques is unknown and further studies are required. The appearance of Δ_1 coherence peaks in our point-contact results suggests that there should be a Fermi surface instability as-

sociated with the AFM transition, where an opened AFM gap modifies the density of states around the Fermi level in a mean-field manner for the abnormal AFM orders in both $CeRu_2Al_{10}$ and $CeOs_2Al_{10}$. A drastic drop of the thermopower $S(T)$ from 30 μV/K to −7 μV/K crossing T_N has been observed only along the *b* axis, also signaling a partial loss of the Fermi surface in the hybridized band around T_N.[33]

Our directional PCS results on $CeRu_2Al_{10}$ support the largest AFM gap along the *b*-axis in the same direction as the AFM propagation vector $\boldsymbol{K} = (0,1,0)$, while the weakest PCS AFM peak intensity is along the *c*-axis parallel to the ordered magnetic moment. In an itinerant SDW scenario of the AFM order, these observations can be naturally explained by the anisotropic c–f hybridization effect, where the *ab*-plane hybridization induces a Fermi surface instability connected by the propagation vector $\boldsymbol{K} = (0,1,0)$ and thus yields an AFM transition. Meanwhile, the *c*-axis magnetic moment is not screened due to a weaker hybridization in this direction considering the small ordered magnetic moment $\mu \sim 0.42\ \mu_B$ in $CeRu_2Al_{10}$. The Ce 4f electrons in $CeRu_2Al_{10}$ are supposed to be more localized with a larger magnetic moment and less hybridized with a smaller T_N than $CeOs_2Al_{10}$.[17] In addition, the opening of a new hybridization gap Δ_h has been observed for both compounds, leading to a metallic nature and interrupting the initial Kondo semiconducting behaviors at low temperatures. Our PCS results on Δ_h are consistent with the claimed V_2 in break-junction tunneling measurements.[31,32]

4. Conclusion

The anomalous AFM phase in $CeRu_2Al_{10}$ and $CeOs_2Al_{10}$ has been investigated by the soft point-contact spectroscopy. Two sets of double-peak spectra have been observed at low temperatures below T_N on both compounds. The symmetric double-peak feature has been ascribed to a moderately anisotropic mean-field gap Δ_1 and is probably associated with an AFM gap in an itinerant SDW scenario due to the c–f hybridization. In addition, an opening of a new c–f hybridization gap may be a common behavior in such systems with Fermi surface instability. More careful studies are required to clarify the origin of the AFM state and its feedback effect on the c–f hybridization in the Kondo semiconductors $CeRu_2Al_{10}$ and $CeOs_2Al_{10}$.

Acknowledgment

We thank J. Kawabata and K. Hayashi for the preparation of single-crystalline samples of $CeOs_2Al_{10}$.

References

[1] Riseborough P S 2000 *Adv. Phys.* **49** 257
[2] Muro Y, Motoya K, Saiga Y and Takabatake T 2009 *J. Phys. Soc. Jpn.* **78** 083707
[3] Kawamura Y, Edamoto S, Takabatake T, Nishioka T, Kato H, Matsumura M, Tokunaga Y, Kambe S and Yasuoka H 2010 *J. Phys. Soc. Jpn.* **79** 103701
[4] Strydom A M 2009 *Physica B* **404** 2981
[5] Nishioka T, Kawamura Y, Takesaka T, Kobayashi R, Kato H, Matsumura M, Kodama K, Matsubayashi K and Uwatoko Y 2009 *J. Phys. Soc. Jpn.* **78** 123705
[6] Khalyavin D D, Hillier A D, Adroja D T, Strydom A M, Manuel P, Chapon L C, Peratheepan P, Knight K, Deen P, Ritter C, Muro Y and Takabatake T 2010 *Phys. Rev. B* **82** 100405
[7] Robert J, Mignot J M, André G, Nishioka T, Kobayashi R, Matsumura M, Tanida H, Tanaka D and Sera M 2009 *Phys. Rev. B* **82** 100404
[8] Kato H, Kobayashi R, Takesaka T, Nishioka T, Matsumura M, Kaneko K and Metoki N 2011 *J. Phys. Soc. Jpn.* **80** 073701
[9] Strigari F, Willers T, Muro Y, Yutani K, Takabatake T, Hu Z, Chin Y Y, Agrestini S, Lin H -J, Chen C T, Tanaka A Haverkort M W, Tjeng L H and Severing A 2012 *Phys. Rev. B* **86** 081105
[10] Kunimori K, Nakamura M, Nohara H, Tanida H, Sera M, Nishioka T and Matsumura M 2012 *Phys. Rev. B* **86** 245106
[11] Thiede V M T, Ebel T and Jeitschko W 1998 *J. Mater. Chem.* **8** 125
[12] Zenou V Y, Meshi L and Fuks D 2011 *Intermetallics* **19** 713
[13] Kobayashi R, Kawamura Y, Nishioka T, Matsumura M, Kodama K, Tanida H, Sera M, Matsubayashi K and Uwatoko Y 2011 *J. Phys. Soc. Jpn.* **80** SA044
[14] Tanida H, Tanaka D, Sera M, Tanimoto S, Nishioka T, Matsumura M, Ogawa M, Moriyoshi C, Kuroiwa Y, Kim J E, Tsuji N and Takata M 2011 *Phys. Rev. B* **84** 115128
[15] Muro Y, Kajino J, Onimaru T, Takabatake T 2011 *J. Phys. Soc. Jpn.* **80** SA021
[16] Kimura S, Iizuka T, Miyazaki H, Irizawa A, Muro Y, Takabatake T 2011 *Phys. Rev. Lett.* **106** 056404
[17] Kimura S, Iizuka T, Miyazaki H, Hajiri T, Matsunami M, Mori T, Irizawa A, Muro Y, Kajino J and Takabatake T 2011 *Phys. Rev. B* **84** 165125
[18] Hayashi K, Umeo K, Takeuchi T, Kawabata J, Muro Y and Takabatake T 2017 *Phys. Rev. B* **96** 245130
[19] Zhang J H, Hu S L, Zhao H C, Wang P, Strydom A M, Luo J L, Steglich F and Sun P J 2016 *Phys. Rev. B* **94** 235120
[20] Tanida H, Tanaka D, Sera M, Moriyoshi C, Kuroiwa Y, Takesaka T, Nishioka T, Kato H and Matsumura M 2010 *J. Phys. Soc. Jpn.* **79** 083701
[21] Kondo A, Kindo K, Nohara H, Nakamura M, Tanida H, Sera M and Nishioka T 2017 *J. Phys. Soc. Jpn.* **86** 023705
[22] Park W K, Tobash P H, Ronning F, Bauer E D, Sarrao J L, Thompson J D and Greene L H 2012 *Phys. Rev. Lett.* **108** 246403
[23] Park W K, Sarrao J L, Thompson J D and Greene L H 2008 *Phys. Rev. Lett.* **100** 177001
[24] Che L Q, Le T, Xu C Q, Xing X Z, Shi Z X, Xu X F and Lu X 2016 *Phys. Rev. B* **94** 024519
[25] Naidyuk Yu G and Yanson I K 1998 *J. Phys.: Condens. Matter* **10** 8905
[26] Newns D M and Read N 1987 *Adv. Phys.* **36** 799
[27] Maltseva M, Dzero M and Coleman P 2009 *Phys. Rev. Lett.* **103** 206402
[28] Zhang X H, Butch N P, Syers P, Ziemak S, Greene R L and Paglione J 2013 *Phys. Rev. X* **3** 011011
[29] Naidyuk Yu G, Kvitnitskaya O E, Jansen A G M, Geibel C, Menovsky A A and Wyder P 2000 *Physica B* **284-288** 1293
[30] Fano U 1961 *Phys. Rev.* **124** 1866
[31] Kawabata J, Ekino T, Yamada Y, Sakai Y, Sugimoto A, Muro Y and Takabatake T 2015 *Phys. Rev. B* **92** 201113
[32] Kawabata J, Ekino T, Yamada Y, Okada Y, Sugimoto A, Muro Y and Takabatake T 2017 *Phys. Rev. B* **95** 035144
[33] Yamada Y, Kawabata J, Onimaru T and Takabatake T 2015 *J. Phys. Soc. Jpn.* **84** 084705